The representation of two phase fault-rock properties in flow simulation models

T. Manzocchi[1], A.E. Heath[2], J.J. Walsh[1] and C. Childs[1]

[1]*Fault Analysis Group, Department of Geology, University College Dublin, Dublin 4, Ireland (e-mail: fault@fag.ucd.ie)*

[2]*Fault Analysis Group, Department of Earth Sciences, University of Liverpool, Liverpool L69 3BX, UK*

ABSTRACT: Faults are represented conventionally in production flow simulation models using transmissibility multipliers which capture the single phase, but not the two phase, fault-rock properties. Available data indicate that fault-rocks have similar two phase properties to sediments of the same permeability, hence existing methods can be applied to estimate two phase fault-rock properties from their intrinsic permeabilities. Two methods of representing the two phase fault-rock properties implicitly in the flow simulator are compared, using one-dimensional numerical flow models containing water-wet faults with imbibition capillary pressure curves. The method which is the closer two phase analogue of the single phase transmissibility multiplier is inappropriate, as the implementation is unreasonably unwieldy. A simpler implementation is to derive pseudo-relative permeability functions including the fault-rock properties in the upstream grid block; these properties are then incorporated directly in the simulator. Relative transmissibility multiplier functions can be back-calculated from the pseudo-relative permeability functions, and indicate how closely the single phase multiplier approximates two phase flow through the fault. Implementation in a 3D model with complex fault juxtapositions validates the approach, and a practical workflow for the routine inclusion of two phase fault-rock properties in conventional faulted flow simulation models is outlined.

KEYWORDS: *fault (geology), relative permeability, capillary pressure, flow model*

INTRODUCTION

Whilst it is routine to consider two phase fault-rock properties in exploration fault seal analysis, these properties are seldom included in production flow simulation models, and there is no straightforward method for doing so. Grid block two phase properties included in flow simulators are relative permeability and capillary pressure functions indexed to the saturation of the grid blocks to which they are attached. As faults are conventionally represented in simulation models as 2D interfaces between grid blocks, no explicit information about fault-rock saturation is included. Therefore, unlike single phase fault properties (fault-rock permeability and thickness) which can be included using dimensionless transmissibility multipliers, two phase fault-rock capillary pressure and relative permeability curves cannot be incorporated directly into the simulator. A method for including two phase fault-rock properties as a function of the upstream grid block saturation is presented, by introducing the concept of the relative transmissibility multiplier.

The fault property and flow conceptualizations made in migration and in production flow modelling are compared on Figure 1. The most important fault property for migration and accumulation studies is the capillary threshold pressure of the fault-rock. Buoyancy driven oil migration is stopped by a fault, and an accumulation forms behind it. As the accumulation grows, the capillary pressure in the carrier-bed adjacent to the fault increases. Eventually, the capillary pressure in the accumulation will match the capillary threshold pressure of the fault, allowing migration through the fault, and limiting the height of the fault-bounded accumulation. This treatment assumes that sufficient time is available for the system to be in equilibrium and hence for flow-related forces to be negligible. It is, therefore, a static treatment. The only significant fluid property is capillary pressure, and the only significant fault property is the fault-rock capillary threshold pressure. This migration conceptualization is used to estimate fault-rock capillary threshold pressures from known column heights (e.g. Gibson 1994; Fristad *et al.* 1997) allowing calibration of forward models to test undrilled potential fault-bounded accumulations (e.g. Childs *et al.* 2002).

The treatment of faults in production simulators differs entirely. The goal of successful production is to maximize flow by exploiting or applying pressure gradients. The resistance to flow is the viscosity of the fluid, and the coefficients relating viscosity and pressure gradient to flow rate, are permeability and length. Hence the most important fault properties for production are the permeability and thickness of the fault-rock, and these properties are captured in the flow simulator as transmissibility multipliers (e.g. Manzocchi *et al.* 1999). Transmissibility multipliers represent a single phase treatment of the fault, as the multiplier acts indiscriminately on all fluid phases. Determining the precise circumstances in which two phase fault-rock properties might be significant in production simulation is outwith the scope of this contribution, which aims only to describe a method for including their effects. However the general influence of the two phase properties increases as a

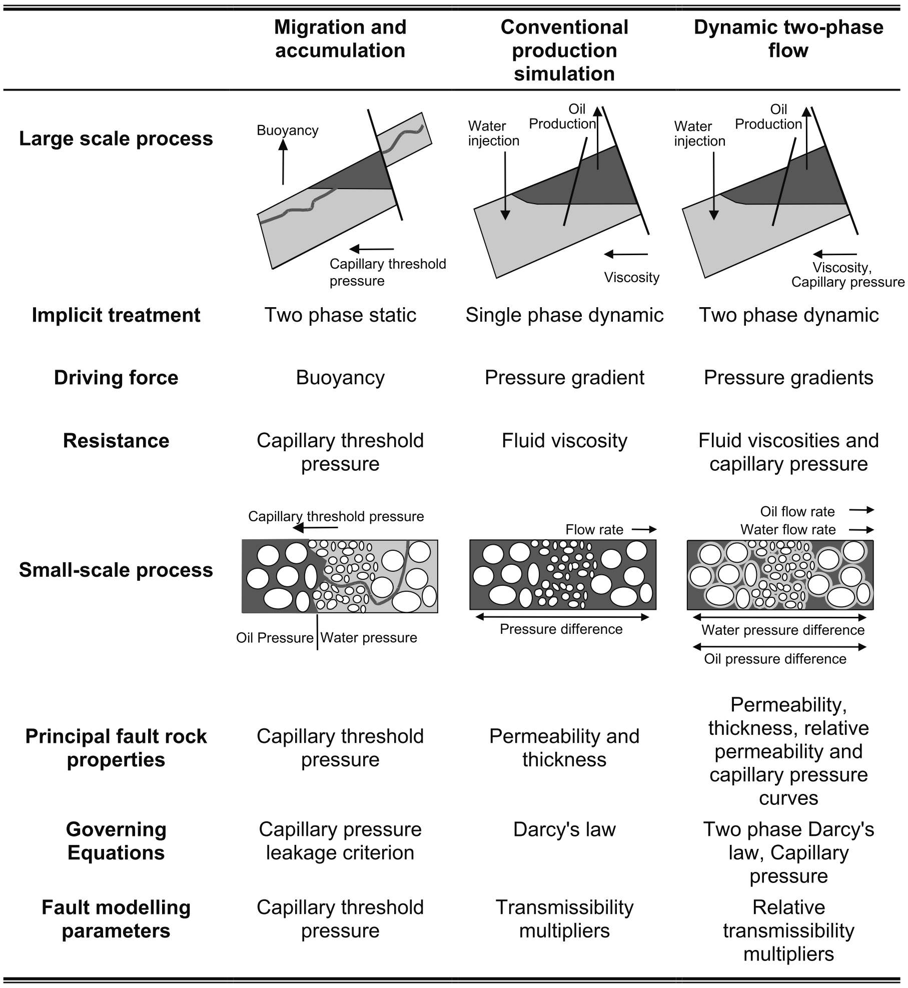

Fig. 1. Comparison of assumptions about flow across faults made in migration studies (Column 1) and conventional production simulation (Column 2). Column 3 combines the conceptualizations made in the two disciplines, and summarizes the factors needing consideration for two phase representation of faults in production simulation. Light grey, water; dark grey, oil.

function of the relative significance of capillary forces to viscous forces present. Capillary forces are most significant at smaller length-scales or lower flow rates (e.g. Ringrose *et al.* 1993), and high capillary pressures in low permeability fault-rock may result in high residual oil saturations upstream of faults. At larger scales or higher flow rates, viscous forces are more dominant in two phase flow processes, resulting in less capillary trapping.

Models investigating the influence of scale and of fault system geometry on oil recovery during waterflooding are shown on Figure 2. Water saturation maps after modelling a waterflood at the same frontal advance rate within four geometrically similar systems at different scales are shown; these models are described in more detail by Manzocchi *et al.* (1998). The four systems contain 10 mD faults with explicit two phase fault-rock properties, embedded in 1D host-rock using discrete grid blocks to represent the faults. Each model has an identical geometrical arrangement of faults and identical single phase equivalent permeabilities. The recovery in the largest system (Fig. 2d), is approximately twice that of the smallest system (Fig. 2a), in which abundant residual oil is trapped behind the faults. The models therefore show an increase in recovery with an increase in scale, illustrating the scale-dependence of capillary effects. A similar dependence exists with respect to flow rate. As scale increases from pore scale to reservoir scale, or as flow rate increases from exploration timescales to production timescales, the overall dependence on capillary properties is reduced; however, there exist scales and flow rates relevant to production in which two phase fault-rock properties may still influence reservoir flow.

Methods for addressing dynamic, two phase fault properties for migration studies are emerging (e.g. Heum 1996), but to date the only fault representation available for production simulation is the single phase transmissibility multiplier. Had the systems in Figure 2 been modelled using only single phase transmissibility multipliers for the faults, then the saturation maps would all be similar to Figure 2d, with similar recoveries at each scale. We show in this paper that two phase fault-rock properties can be accurately represented in conventional flow simulation models, without representing the faults as discrete grid blocks. The closest two phase analogue of the single phase transmissibility multiplier is derived, but cannot be implemented in conventional simulators. However, a less direct analogue can be used, and is determined from the relative permeability pseudo-functions (e.g. Kyte & Berry 1977; Corbett & Jensen 1993) including effects of the fault-rock in the upstream grid block. The ratio of the pseudo-relative permeability, to grid block relative permeability, defines the relative transmissibility multiplier for each fluid phase.

An alternative approach to the problem is to represent fault-rock in flow models using discrete grid blocks, as in the models described above (Fig. 2). Although this approach is appealing, as it additionally allows incorporation of a much broader range of single phase fault-rock properties than is possible by representing the faults as 2D interfaces (e.g. along-fault flow within anisotropic fault-zones; Evans *et al.* 1997; Faulkner & Rutter 1998), the principal drawback is the

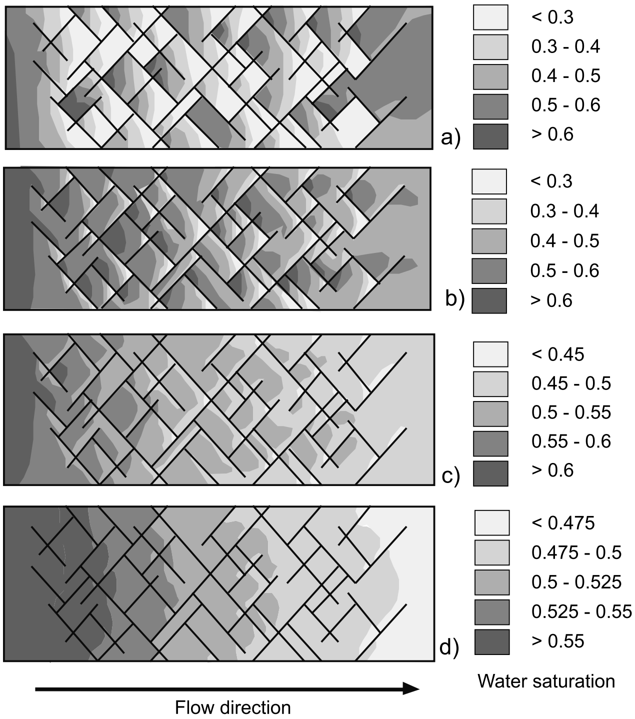

Fig. 2. Results from waterflooding a geometrically similar fault system at different scales. Maps of water saturation after two pore volumes of water injected at a Darcy velocity of 1 ft day^{-1}. Model length is (**a**) 3 m, (**b**) 30 m, (**c**) 300 m and (**d**) 3 km, and the faults are 1 mm, 1 cm, 10 cm and 1 m thick. Matrix permeability is 1000 mD, and fault permeability is 10 mD. Fault-rock is represented as discrete grid blocks and the capillary pressure and relative permeability curves used for both fault-rock and matrix are determined from the relationships given by Ringrose *et al.* (1993). Total recovery in the largest model is about twice that in the smallest model, due to capillary trapping in small compartments.

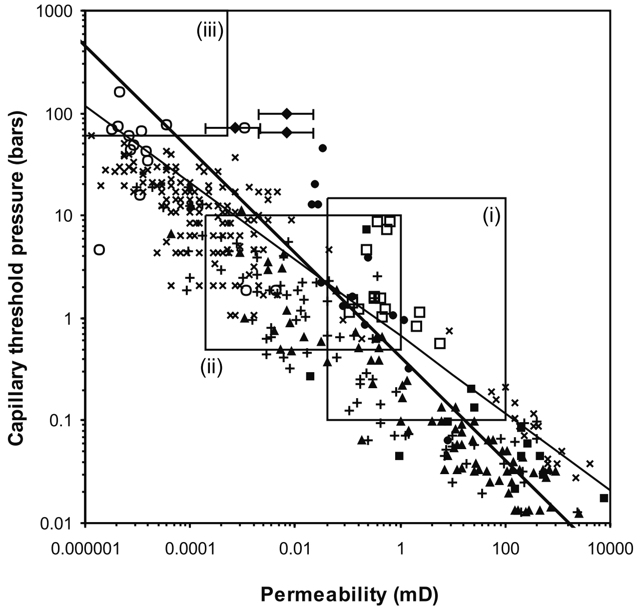

Fig. 3. Capillary threshold pressure vs. permeability for fault samples (solid symbols) and unfaulted rock samples (crosses and open symbols) from a variety of lithologies. The boxes (Fisher & Knipe 1998) are summaries of data from (i) faults in clean sandstone, (ii) dirty sandstone and (iii) shale-rich fault gouge. The two lines are published model relationships (thinner line from Ringrose *et al.* (1993) and Fisher & Knipe (1998), thicker line from Harper & Lundin (1997)). Capillary threshold pressures have been normalized for a water-wet system with a hydrocarbon–water interfacial tension of 40 dynes cm^{-1}, and a contact angle of 30°. Legend: filled triangles and crosses, Sperrevik *et al.* (2002); filled squares, Harper & Lundin (1997); empty squares, Schowalter (1979); filled circles, Gibson (1998); filled diamonds, Fulljames *et al.* (1997); ×, Ibrahim *et al.* (1970); empty circles, Schlomer & Krooss (1997).

increase in the number of grid blocks required. A single fault grid block (perhaps 10 cm wide) within a full-field simulation model in which grid blocks are approximately four orders of magnitude wider, results in severe numerical difficulties for the simulator. Extremely small time-steps are required to achieve convergence of numerical solutions in these circumstances, resulting in lengthy simulator run-times. These run-times can be shortened and numerical artefacts reduced, if the faults, and the grid blocks adjacent to the faults, are more finely discretized. This, however, can result in impractically large simulation models for complex faulted reservoirs.

TWO PHASE FAULT-ROCK PROPERTIES

Published laboratory analyses of two phase fault-rock properties are generally limited to values of capillary threshold pressure, the most significant parameter for exploration fault-seal analysis, although occasional mercury intrusion capillary pressure curves over the full saturation range have been published (e.g. Pittman 1981; Knipe *et al.* 1997). Figure 3 gives a summary of available capillary threshold pressure data for faults, normalized for a moderately water-wet oil–water system (40 dynes cm^{-1} interfacial tension; 30° contact angle), cross-plotted against fault permeability. Higher permeability faults have threshold pressures similar to unfaulted rock, and although clay-rich fault-rock values are somewhat higher than unfaulted rock with the same permeability, given the scarcity of published capillary threshold pressure data for low permeability fault-rocks, this observation is tentative. For qualitative modelling purposes, therefore, the relationship between threshold pressure and permeability for both fault-rock and unfaulted sediments can be considered the same (Fig. 3). This conclusion is supported by the similarity of the two lines on the plot, which represent model predictions of capillary threshold pressure for fault-rock (thicker line; Harper & Lundin 1997) and for sediments (thinner line). The model curve for sediments is derived from the function defined in Ringrose *et al.* (1993):

$$Pc = C' S_e^{-2/3} (\varphi/k)^{0.5} \quad (1)$$

where $C' = 3$ gives capillary pressure in bars, φ is porosity, k is absolute (single phase) permeability in mD, and S_e is the effective wetting phase saturation. S_e is defined as:

$$S_e = (S_w - S_{wc})/(S_{wor} - S_{wc}), \quad (2)$$

where S_w is water saturation, S_{wc} is the connate water saturation, and S_{wor} is the water saturation at irreducible oil. S_e takes a value of 1 to define the capillary threshold pressure. Fault-rock porosity has been determined from permeability using the empirical relationship $\varphi = 0.05k^{0.25}$, which provides a reasonable fit, albeit with a wide scatter, to published (Pittman 1981; Fowles & Burley 1994; Berg & Avery 1995; Evans *et al.* 1997; Knipe *et al.* 1997; Fisher & Knipe; 1998) and unpublished fault-rock data.

Given that fault-rock and sediment capillary threshold pressures for rocks with similar permeabilities are similar (Fig. 3), then the absolute permeability based relative permeability and capillary pressure functions applied to sediments (Ringrose *et al.* 1993) can also be applied to fault-rocks. For the simulation models described in this study, we use these functions, with a few modifications. First, we determine fault-rock porosity as a function of absolute permeability, as outlined above. Second, we use a higher value for S_{wor} ($S_{wor} = 0.85$ rather than 0.6). Third, we change the function defining the connate water saturation, to

$$S_{wc} = 0.85 - 10^{(-0.6\exp(-0.5\log(k)))} \tag{3}$$

This change, which has no theoretical basis whatsoever, has been made to ensure non-zero effective saturation ranges for lower permeability rock. Finally, in addition to equation (1) to define the drainage capillary pressure curve, we use the relationship

$$p_c = C'(1 - S_e^{5})S_e^{-2/3}(\varphi/k)^{0.5} \tag{4}$$

to define an imbibition capillary pressure curve. The water and oil relative permeability (k_{rw} and k_{ro} respectively) curves used are identical to those defined by Ringrose *et al.* (1993). These are

$$k_{rw} = 0.3S_e^{3} \tag{5}$$

and

$$k_{ro} = 0.85(1 - S_e)^{3} \tag{6}$$

Resultant capillary pressure and relative permeability curves for 0.01 mD and 10 mD fault-rock are shown on Figure 4.

The methods outlined above provide two phase model input for fault-rocks as a function of the absolute fault-rock permeability. The two critical fault-rock variables which influence the single phase fault transmissibility multiplier are the absolute fault-rock permeability and the fault-rock thickness (e.g. Walsh *et al.* 1998; Manzocchi *et al.* 1999). Where subsurface data are unavailable, these must be estimated, and predictive proprietary algorithms specific to particular hydrocarbon provinces or fields are used for this purpose. The most significant fault permeability determinants appear to be the fault-rock shale content and the depth at time of faulting (Fisher & Knipe 1998; Manzocchi *et al.* 1999; Sperrevik *et al.* 2002; Yielding 2002). Once a prediction is available for the single phase, absolute permeability of the fault-rock, the functions defined above can be used to determine complementary two phase fault-rock properties. One further choice has to be made: whether to use the drainage or the imbibition capillary pressure curve.

The capillary threshold pressure of a fault-rock represents the capillary pressure required for a non-wetting phase to form a connected flow-path through the rock. If the capillary threshold pressure has been exceeded, both oil and water are mobile phases within the fault-rock, and the fault-rock water saturation will be determined by the local capillary pressure and by the shape of the fault-rock capillary pressure curve. Water-flooding, a typical hydrocarbon recovery process and the one considered in this study, is generally considered an imbibition process in which the wetting phase (water) displaces the non-wetting phase (oil). Provided the local capillary pressure exceeds the fault-rock capillary threshold pressure, then the saturation in the fault-rock will be between S_{wc} and S_{wor},

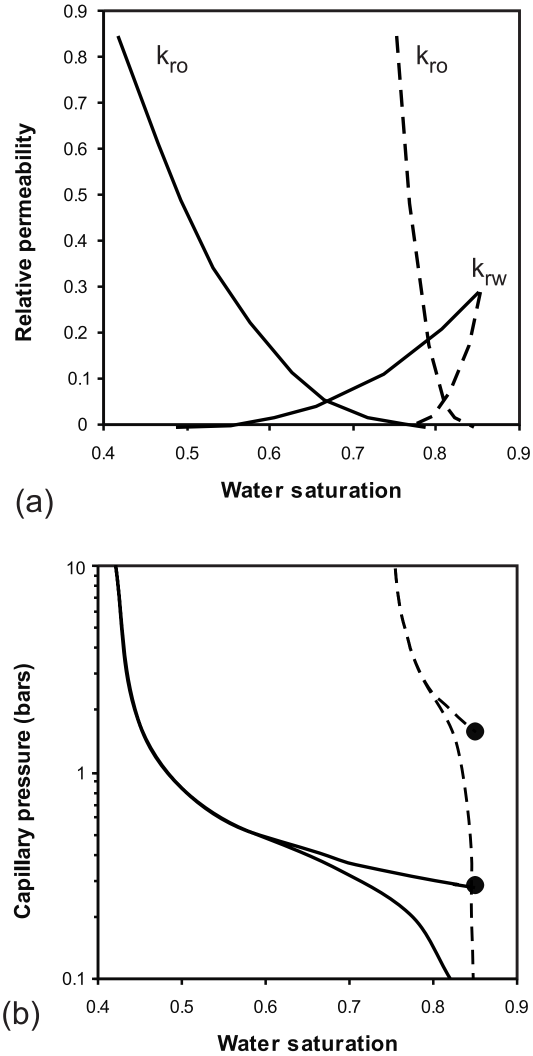

Fig. 4. (**a**) Synthetic relative permeability and (**b**) capillary pressure curves for 0.01 mD (dashed lines) and 10 mD (solid lines) fault-rock. The black circles on (b) mark the capillary threshold pressure on the drainage capillary pressure curves. At this saturation (S_{wor}) the oil relative permeability and the imbibition capillary pressure both go to zero.

and the imbibition fault-rock capillary pressure curve is appropriate. If, on the other hand, the capillary pressure in the reservoir-rock adjacent to the fault is lower than the fault-rock capillary threshold pressure, then the fault-rock water saturation remains above S_{wor}, the fault is impermeable to oil, and the drainage capillary pressure curve is appropriate. A fault in this situation can only become permeable to oil if the capillary pressure adjacent to the fault is in some way increased, possibly through a mechanism similar to water-drive leakage discussed by Heum (1996).

For the models described in the present study, imbibition capillary pressure curves are used throughout. This implies that that there is mobile oil in the faults throughout the simulation runs. The faults in these models are therefore less detrimental to flow of oil than if drainage curves were applied to the faults. The further a fault is above the oil–water contact, the greater the probability that the fault-rock capillary threshold pressure has been exceeded, and therefore faults lower in the reservoir will be, in general, more detrimental to across-fault oil flow than faults higher in the reservoir.

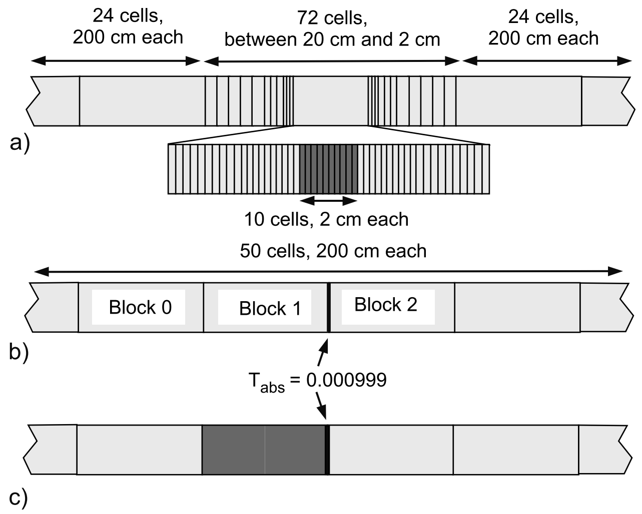

Fig. 5. Cartoon of the flow simulation models used to illustrate the methods developed to represent two phase fault-rock properties. (**a**) Fine-scale model incorporating a discrete thickness of low permeability fault-rock (darker cells). The grid blocks get gradually smaller approaching the fault in order the minimize numerical artefacts. (**b**) Coarse model in which the fault is represented using a single phase transmissibility multiplier T_{abs}. Blocks 0, 1 and 2 are grid blocks referred to in the text. (**c**) Coarse model in which the fault is represented using T_{abs}, and using pseudo-relative permeability functions in the upstream grid block to represent the two phase fault-rock properties (darker cell). Flow is from left to right.

THE REPRESENTATION OF TWO PHASE FAULT-ROCK PROPERTIES USING RELATIVE TRANSMISSIBILITY MULTIPLIERS

This section describes possible approaches for including the two phase properties of fault-rock in conventional faulted flow simulator models as phase-specific transmissibility multipliers. After reviewing the single phase transmissibility multiplier, we derive a direct, two phase analogue. It is shown that this analogue cannot be implemented directly, as the phase transmissibility multiplier is a property of the interface between grid blocks, yet is also dynamic. As it is a dynamic property, it must be indexed to the saturation of a grid block; the most appropriate grid block being the one upstream of the fault. This results in an impractical function which depends on two different, but overlapping, saturation averaging volumes. The problem may be treated much more simply by deriving an appropriate grid block pseudo-relative permeability function, which includes the properties of the upstream grid block and of the fault-rock. Practical, but not completely analogous, two phase versions of the single phase transmissibility multiplier may then be back-calculated from the grid block oil and water pseudo-relative permeability functions.

In the discussion, grid block dips are ignored, the grid block net: gross ratios and the across-fault grid block to grid block juxtaposition areas are all taken as unity, and all non-fault grid blocks have the same properties. These parameters influence transmissibilities and transmissibility multipliers, but we make these simplifications to focus on the permeabilities, lengths and two phase properties of the fault-rock. The methods discussed are illustrated using flow simulation results for a 1D waterflood across a 20 cm thick, 0.1 mD fault contained within 2 m long, 1000 mD grid blocks, with a Darcy velocity of 0.01 ft day^{-1}. Water and oil viscosities are 1 cp and 5 cp respectively. Simulation results are compared for models in which the fault is represented using discrete grid blocks (Fig. 5a), using the single phase fault transmissibility multiplier (Fig. 5b) and using the single phase fault transmissibility multiplier complemented by phase-specific relative transmissibility multipliers (Fig. 5c). The relative transmissibility multipliers are defined as the phase-specific transmissibility multipliers normalized by the single phase transmissibility multiplier, a definition analogous to that of relative permeability (phase-specific effective permeability normalized by single phase intrinsic permeability).

The absolute transmissibility multiplier

Transmissibility multipliers are used in flow simulation specifically to overcome the problem addressed in this paper: the implicit representation of a thickness of low permeability rock (typically horizontal shales or sub-vertical faults) without using explicit grid blocks. Using the simplifications described above, the transmissibility between two grid blocks is the harmonic average permeability between the grid block centres, normalized by the distance separating them. Therefore, if there are n discrete permeability regions separating the grid block centres, the transmissibility is:

$$Trans = \left[\sum_{i=1}^{i=n} \frac{L_i}{k_i} \right]^{-1} \tag{7}$$

Where k_i is the permeability, and L_i is the length, of each permeable region. The absolute, single phase transmissibility multiplier (T_{abs}) is the ratio of the transmissibility between two grid blocks calculated by including the fault-rock (typically $n=3$), against that calculated by excluding it ($n=2$).

Therefore, for two grid blocks of lengths L_1 and L_2, and permeabilities k_1 and k_2, separated by a fault of permeability k_f and thickness t_f, the absolute transmissibility multiplier can be derived from equation (7), and is (Manzocchi *et al.* 1999):

$$T_{abs} = \left[1 + t_f \left(\frac{2/k_f - 1/k_1 - 1/k_2}{L_1/k_1 + L_2/k_2} \right) \right]^{-1} \tag{8}$$

The phase transmissibility multiplier

The effective phase permeability in two phase flow is the product of the single phase, absolute permeability k, and the saturation-dependent relative permeability k_{rp}, where phase p is oil or water. Therefore, following equation (7), the phase transmissibility between two grid blocks, is:

$$Trans_p = \left[\sum_{i=1}^{i=n} \frac{L_i}{k_i k_{rpi}} \right]^{-1} \tag{9}$$

where k_{rpi} is the relative permeability of region i. Figure 6 shows saturation profiles at three discrete times during the example simulated waterflood. As saturation changes as a function of both time and distance, the relative permeabilities along the profile also change during the course of the simulation. Therefore equation (9) cannot be simplified in a similar manner to equation (7), as it is saturation dependent via the k_{rp} term. A two phase analogy to T_{abs} must therefore be determined from the flow simulation results. By direct analogy with the single phase transmissibility multiplier, the two phase transmissibility multiplier (T_p) can be defined as the phase specific ratio of transmissibility between the centres of block 1 and 2 including and excluding the fault properties.

Transmissibility including the fault properties is given by equation (9). The phase transmissibility excluding the fault

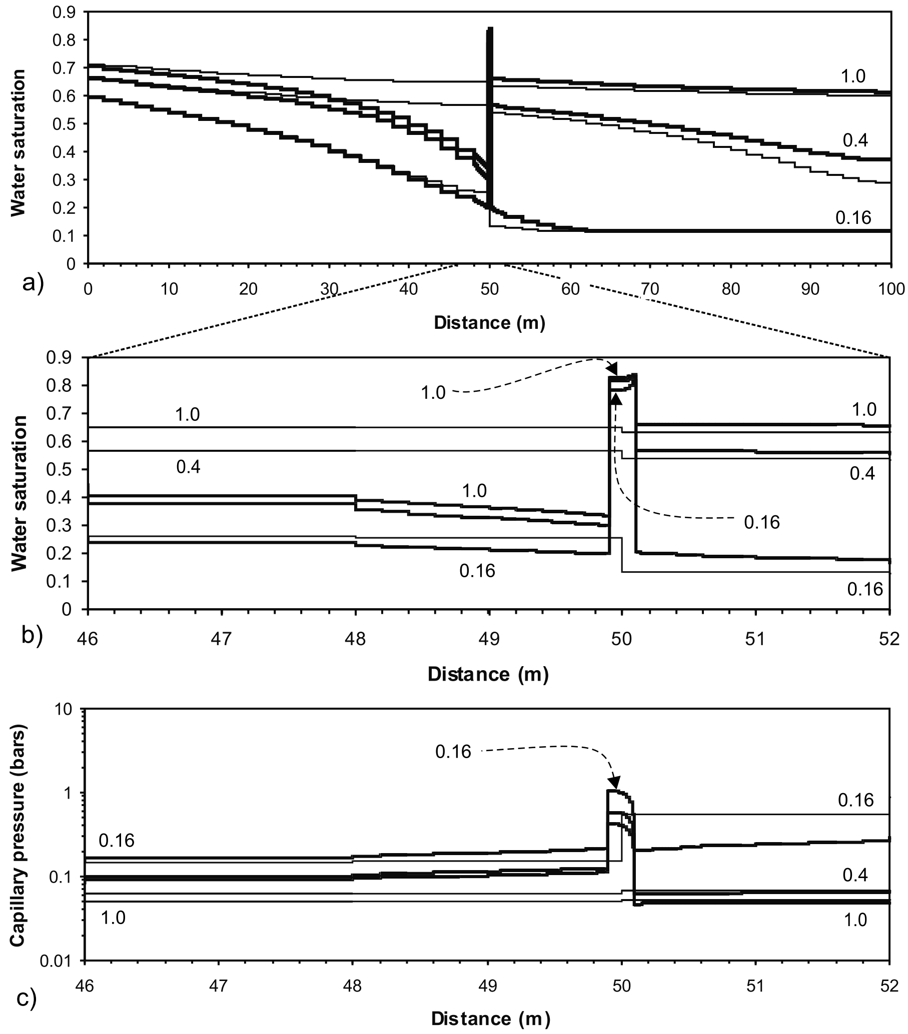

Fig. 6. (**a**, **b**) Water saturation and (**c**) capillary pressure profiles at 0.16, 0.4 and 1 pore volumes of injected water, for the example model. Flow direction is left to right. (a) shows the whole model, while (b, c) show coarse blocks 0 to 2. Thicker lines: fine model with explicit fault-rock properties. Thinner lines: coarse model with only T_{abs}. The low water saturation observed upstream of the fault in the fine model indicates trapped oil which is not reproduced in the coarse model. This oil is trapped as the capillary pressure in the faults remains high even late in the simulation run (c). The higher water saturations observed downstream of the fault in the fine model are a function of the imposed constant Darcy velocity boundary conditions: trapped oil, coupled with a constant water injection rate, implies that more water has passed through the fault at the same volume of injected water, so water saturations downstream of the fault are necessarily higher.

properties (in the case where k_1 and k_2 are the same) is given by:

$$Trans_{p(\text{no fault properties})} = 2k_e k_{\mathrm{rp}(\bar{S}_{\mathrm{w}})}/(L_1 + L_2) \tag{10}$$

where k_e is the permeability of the two grid blocks and $k_{\mathrm{rp}(\bar{S}_{\mathrm{w}})}$ is the relative phase permeability of the grid blocks at a saturation $\bar{S}_{\mathrm{w}}$. $\bar{S}_{\mathrm{w}}$ is the porosity weighted average saturation obtained between grid block centres in the model run with explicit two phase fault-rock properties, given by:

$$\bar{S}_{\mathrm{w}} = \sum_{i=1}^{i=n} L_i \varphi_i S_{\mathrm{w}i} \Big/ \sum_{i=1}^{i=n} L_i \varphi_i \tag{11}$$

The phase transmissibility multiplier is then given by:

$$T_p(\bar{S}_{\mathrm{w}}) = \frac{Trans_{p(\text{equation 9})}}{Trans_{p(\text{equation 10})}} \tag{12}$$

Figure 7 shows the resultant oil and water phase transmissibility multipliers as a function of injected water. From this graph it is clear not only that different transmissibility multipliers should be assigned to the different phases present, but that these phase-specific multipliers should also change during the course of the simulation run. The saturation profiles obtained in the fine-scale model with explicit two phase fault-rock properties could only be reproduced in a coarse-scale model if dynamic phase transmissibility multipliers (T_p) were to replace T_{abs}. Below we discuss how T_p can be included in

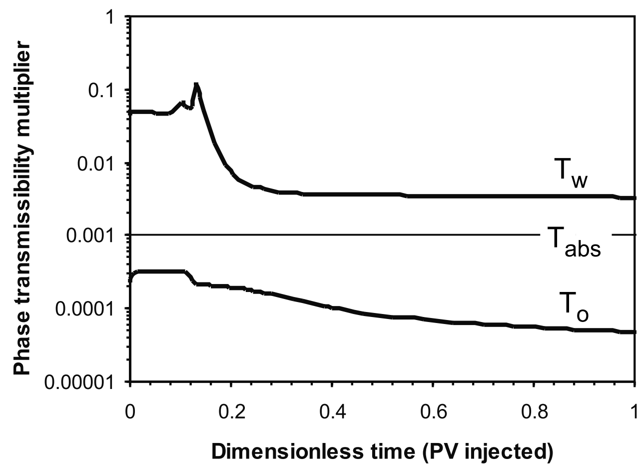

Fig. 7. Water and oil phase transmissibility multipliers as a function of dimensionless time (pore volumes of injected water) for the example model. Oil transmissibility is consistently lower than the single phase multiplier accounts for, and water transmissibility consistently higher. The precise magnitude of the discrepancy varies as a function of time.

the flow calculation performed by the simulator in a coarse model.

The relative transmissibility multiplier as a direct analogue with the single phase multiplier

In many simulators, including the Eclipse simulator used in this study (Schlumberger Geoquest 1999), the phase specific flow rate (q_p) between grid blocks 1 and 2 is given by:

$$q_{p12} = T_{12}T_{\mathrm{abs}}\frac{k_{\mathrm{rp1}}}{\mu_p}dP_p, \tag{13}$$

where T_{12} is the absolute (i.e. single phase) transmissibility between the blocks, T_{abs} is the absolute transmissibility multiplier, μ_p is phase viscosity, dP_p is the phase pressure difference between the block centres, and, significantly, k_{rp1} is the relative permeability of the upstream grid block. The significance of this upstream relative permeability weighting is discussed in the following section. Equation (13) does not give the correct phase fluxes through the fault, as T_{abs} should be replaced by T_p (Figs 6,7). By normalizing T_p against T_{abs}, and reformulating it as a function of the water saturation in the upstream grid block (S_{w1}), the relative transmissibility multipliers $T_{\mathrm{rp}(S_{\mathrm{w1}})}$ can be obtained. Thus:

$$T_{\mathrm{rp}(S_{\mathrm{w1}})} = T_{p(\bar{S}_{\mathrm{w}})}/T_{\mathrm{abs}}. \tag{14}$$

Equation (13) can then be modified to include T_{rp}. This gives:

$$q_{p12} = T_{12}T_{\mathrm{abs}}T_{\mathrm{rp}(S_{\mathrm{w1}})}\frac{k_{\mathrm{rp1}}}{\mu_p}dP_p. \tag{15}$$

Both T_{rp} and k_{rp} are now functions of the water saturation of the block immediately upstream of the fault (block 1), and therefore may be combined to give a pseudo-relative permeability function k'_{rp}, where

$$k'_{\mathrm{rp1}} = T_{\mathrm{rp}(S_{\mathrm{w1}})}k_{\mathrm{rp1}}. \tag{16}$$

In this way, equation (15) becomes:

$$q_{p12} = T_{12}T_{\mathrm{abs}}\frac{k'_{\mathrm{rp1}}}{\mu_p}dP_p, \tag{17}$$

which contains the same number of terms as equation (13), but retains the saturation-dependent two phase properties of the fault-rock within the coarse-grid model. $T_{\mathrm{rp}(S_{\mathrm{w1}})}$ and k'_{rp1} are shown as the thicker curves on Figure 8a, b.

The relative transmissibility multiplier as a grid block property

The previous section shows that relative transmissibility multipliers must be incorporated in the simulator flow calculation by defining a pseudo-relative permeability which captures the two phase fault-rock properties in the upstream grid block (equation (16)). Therefore, although the T_p function defined above (equation (12); Fig. 7) is the closest two phase analogy to T_{abs}, it cannot be implemented directly and T_{rp} (equation (14), Fig. 8a) must be derived. T_{rp} is based on two distinct water saturation averaging volumes. The phase transmissibility multiplier (equation (12)) is calculated on the basis of the average saturation between the centres of the upstream and down-

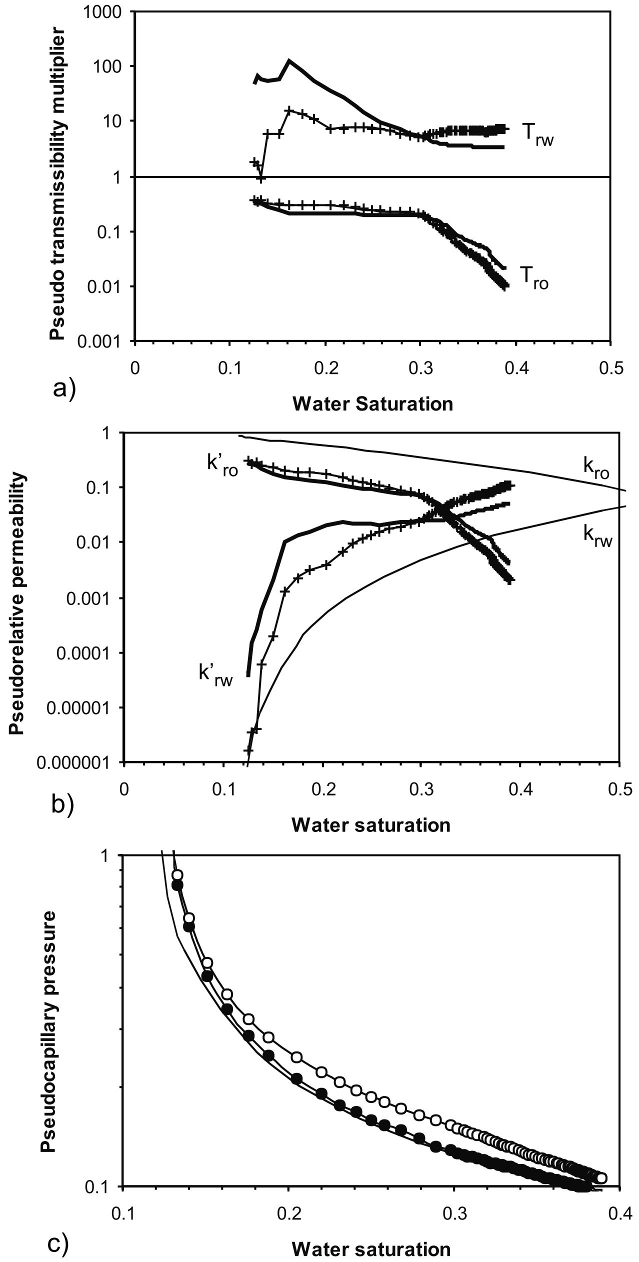

Fig. 8. (**a**) Relative transmissibility multipliers for oil and water as a function of the saturation of the grid block immediately upstream of the fault, for the example model. Thicker curves: T_{rp} calculated from the closest T_{abs} analogue. Thinner curves: T_{rp} calculated from pore volume weighted pseudo-relative permeabilities. Crosses: T_{rp} calculated from Kyte & Berry pseudo-relative permeabilities. (**b**) Pseudo-relative permeabilities for oil and water for the representations shown in (a). Also shown are the parent, grid block relative permeability curves. (**c**) Pseudo-capillary pressure calculated using pore volume weighted pressures (open circles) and Kyte & Berry pressures (filled circles). The unornamented line is the unaltered grid block capillary pressure.

stream grid blocks ($\bar{S}_{\mathrm{w}}$). However, the relative transmissibility multiplier (equation (14)) must be normalized against the upstream grid block saturation (S_{w1}), in order that it be indexed to the same variable as the relative permeability used to calculate flow.

As a consequence of the upstream relative permeability weighting used to calculate flow (equation (13)), the relative transmissibility multiplier is a grid block property, unlike T_{abs}

and T_p which are properties of the interface between grid blocks. Therefore, no direct two phase analogy of the single phase transmissibility multiplier can be implemented in the simulator. T_{rp}, as defined in equation (14), is indexed to the saturation in a whole grid block, but its value depends on half of this grid block, and half of the downstream grid block, as well as on the fault-rock between them. T_{abs} and T_p depend only on the fault-rock and the two half grid blocks.

The reason that many simulators use the relative permeability of the upstream grid block to define the flow between two grid blocks can best be understood by considering the case of a waterflood in which there is no capillary pressure. As the front advances through such a model, the saturation of a grid block immediately downstream of the flood-front is S_{wc}, hence the grid block has zero relative water permeability. The harmonic average equivalent water permeability between this grid block and the one upstream of it is therefore also zero, and so no advance of the waterflood front into the grid block would be possible. Because of such unrealistic artefacts, the upstream grid block relative permeability is used.

The relative transmissibility multiplier from pseudo-relative permeability functions

Recognizing that T_{rp} is a property of the upstream grid block rather than the interface between grid blocks allows the effects of the two phase fault-rock properties to be much more simply determined by calculating the pseudo-relative permeability directly, and back-calculating the relative transmissibility multiplier. Various methods are used for determining relative permeability pseudo-functions; these have been reviewed recently by Barker & Thibeau (1997) and Barker & Dupouy (1999). Christie (2001) differentiates between two basic approaches, termed weighted potential methods (e.g. Kyte & Berry, pore volume weighted) and total mobility methods (e.g. Stone's method).

The present study considers weighted potential methods, in which the pseudo-relative permeability (k'_{rp}) is calculated from the fine-scale flow model using:

$$k'_{\text{rp}} = \frac{\mu_p \bar{q}_p}{T_{12} d\bar{P}_p}, \tag{18}$$

where μ_p is viscosity, $\bar{q}_p$ is the flow rate out of the fault, T_{12} is the transmissibility between the centres of coarse grid blocks 1 and 2 (Fig. 5) which (in the 1D unit cross-sectional area case considered) derives from equation (7), and $d\bar{P}_p$ is an estimate of the pressure difference between the centres of blocks 1 and 2. The pseudo-relative permeabilities are indexed to the saturation of grid block 1 ($\bar{S}_{\text{w1}}$) which derives from equation (11). The effective connate water saturation of the upstream block is taken as the porosity-weighted average S_{wc} of the host-rock and fault-rock.

In the pore volume weighted (PVW) method, the average pressures, $\bar{P}_p$, of the coarse grid blocks is calculated using the same weighting as saturation, i.e:

$$\bar{P}_p = \sum_{i=1}^{i=n} L_i \varphi_i P_{pi} \Big/ \sum_{i=1}^{i=n} L_i \varphi_i \tag{19}$$

In Kyte & Berry's (K&B) method, $\bar{P}_p$ (for the 1D cases considered) is simply the phase pressure recorded in the grid block of the fine-scale model which has its centre in the same place as the centre of the coarse grid block. In both cases, pseudo-capillary pressure for grid block 1 is given by:

$$Pc'_1 = \bar{P}_{\text{o1}} - \bar{P}_{\text{w1}} \tag{20}$$

Although no longer an integral part of the derivation of the pseudo-relative permeability function, the resultant relative transmissibility functions back-calculated from k'_{rp} remain useful devices as they indicate how good an approximation T_{abs} provides to the two phase flow through the fault. k'_{rp} and the back-calculated T_{rp} are shown on Figure 8, which shows that the PVW and K&B k'_{rp} and T_{rp} curves are virtually identical. The main differences between these curves and the curves calculated from equations (14) and (16) (the thicker curves on Fig. 8a, b) is that the weighted potential T_{rw} curves are lower at low water saturation and are less sensitive to water saturation at higher water saturation.

The PVW and K&B pseudo-capillary pressure curves (Fig. 8c) are dissimilar. At low S_{w}, they both have values appreciably higher than the original Pc curve for the grid block, but while the PVW Pc' curve remains higher at higher S_{w}, the K&B curve tends to the unaltered grid block curve.

Discussion of results

Results for various implementations of two phase fault-rock properties are shown on Figure 9, which charts saturations observed in the two coarse grid blocks upstream of the fault (blocks 0 and 1 on Fig. 5) throughout the course of the waterflood. The saturations in these two grid blocks obtained for the conventional representation using only T_{abs} are plotted for comparison on Figure 9a. As expected, the fine scale model run with explicit two phase fault properties has lower saturations in these grid blocks, with the higher residual oil in the block immediately upstream of the fault (block 1).

Results using the pseudos produced as a function of the analogue to the single phase multiplier are shown in Figure 9a. In this representation, the Pc curve of the grid block is not a pseudo-property, as the derivation of k'_{rp} (equations (12), (14), (16)) does not include grid block phase pressures. The coarse model representation results in similar saturations to the fine-scale model at 2PV, but shows too sharp an increase in water saturation until about 0.6 PV, after which the grid block saturations remain virtually unchanged for the remainder of the simulation period. This is because equation (10), used to define these functions, assumes that the saturations are the same in blocks 1 and 2 (Fig. 5) for a model in which the faults are represented only using T_{abs}. Figure 6 shows clear saturation breaks across the fault in such a model. Hence $k_{\text{rp}(\bar{S}_{\text{w}})}$, calculated from the fine-scale model, should not be indexed directly to the unfaulted model to determine $T_{p(\bar{S}_{\text{w}})}$, as per equation (12). Instead, a simulation model including only T_{abs} is required, and the comparison transmissibility should be determined from this model using equation (7), rather than from a completely unfaulted model using equation (12). $T_{p(\bar{S}_{\text{w}})}$ should then be calculated at those times when both the fine-scale, explicit two phase fault model, and the T_{abs} model, have identical saturations ($\bar{S}_{\text{w}}$) in the relevant averaging volume.

The pore volume weighted pseudos (Fig. 9b) honour well the saturations in the block immediately upstream of the fault (block 1), but the saturations calculated for block 0 are too low. By contrast, the saturations obtained from the coarse model containing the Kyte & Berry pseudos (Fig. 9c) provide an extremely close match to the saturations observed in the fine-scale model for both blocks. The PVW pressure average

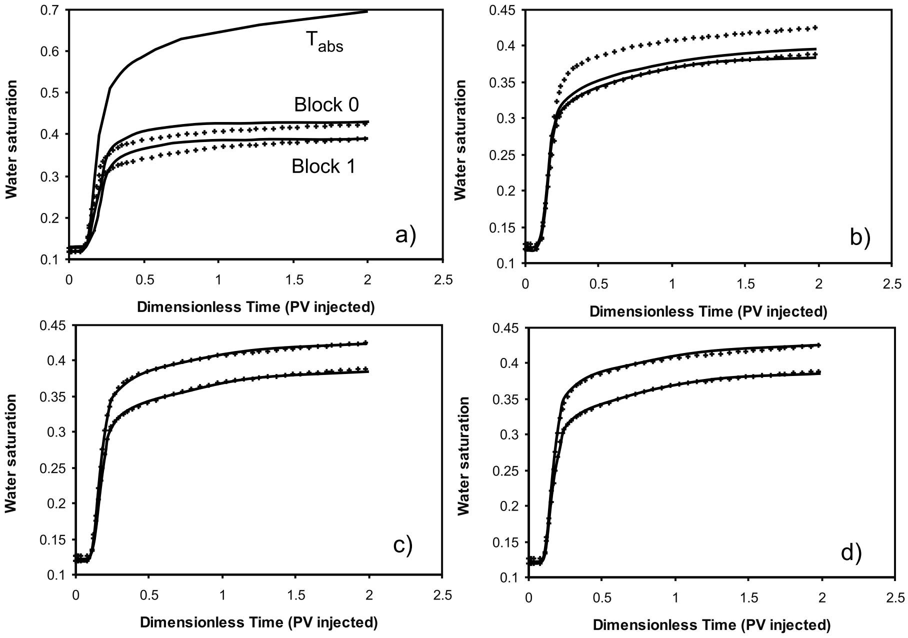

Fig. 9. Water saturation in blocks 0 and 1 (Fig. 5) as a function of pore volumes injected. Crosses: fine model with explicit two phase fault-rock properties. (**a**) Coarse model using k'_{rp} derived from the closest T_{abs} analogue. The curve labelled T_{abs} shows the saturation in these blocks resulting from the conventional coarse representation including the faults as single phase transmissibility multipliers. (**b**) Pore volume weighted pseudo-relative permeability and pseudo-capillary pressure. (**c**) Kyte & Berry pseudo-relative permeability and pseudo-capillary pressure. (**d**) Pore volume weighted pseudo-relative permeability and parent grid block capillary pressure.

(equation (19)) is inappropriate for the geometrical arrangement of fault-rock and reservoir rock present in the model, as the high capillary pressure region of block 1 is thin and occurs at the extreme downstream edge of the block. The PVW pressure average has the effect of smearing this high capillary pressure region throughout block 1, thereby overly restricting oil flow into it from block 0. The K&B Pc' curve, which is very similar at higher S_w to the unaltered Pc curve of the grid block derived from equation (4), gives better results as the pressure averages are more appropriate to the model geometry.

There are problems associated with implementing the Kyte & Berry pseudo-capillary pressures in a 3D model (e.g. Barker & Dupouy 1999), and the method produces directional Pc' which (unlike directional k'_{rp}) cannot be included in the simulator (Schlumberger Geoquest 1999). The conventional representation of faults as transmissibility multipliers places the fault-rock between rather than within grid blocks. Therefore, for flow parallel to the fault (i.e. in the two directions perpendicular to the one considered in these 1D models), the appropriate capillary pressure is the unaltered grid block curve. Figure 9d shows results using the PVW k'_{rp} curves but no pseudo-capillary pressure. The match to the fine-scale model results is not as close as when the K&B Pc' is included but is, none the less, perfectly adequate. Therefore, although directional capillary pressure cannot be implemented, it appears that using the unaltered grid block Pc curve results in an acceptable compromise.

IMPLEMENTATION IN A 3D MODEL

In the previous section we examined, using simple 1D models, possible methods for including two phase fault-rock properties in flow simulation models. We concluded that the most direct two phase analogue of the single phase transmissibility multiplier is impractical, and that the fault-rock can be efficiently included using relative permeability pseudo-functions attached to the upstream grid block. In this section we implement this method in a faulted, 3D model containing complex across-fault juxtapositions. The model is smaller, and the flow rates lower, than might be expected in a producing reservoir – this is so that capillary trapping effects are significant, and that the differences between the various fault representations can be observed more clearly.

Model description

The model is shown on Figure 10, and comprises 7 layers of 1000 mD reservoir-rock interbedded with six impermeable layers. The overall sequence thickness is 25 m, of which 15 m is permeable. The model dimensions are 500 m by 500 m, discretized into 25 m square coarse grid blocks. The model contains two faults; one with a constant 10 m throw, and the other with a throw varying between 5 and 15 m. A water injector and a producer well in opposite corners of the model have a constant, 40 bar pressure differential. Hence the waterflood must pass through at least two faults to get to the producer well. Figure 10b shows an Allan diagram of the faults, with grey-scale coding according to connection permeability. Only connections between permeable grid blocks are shown. Fault permeability, which decreases towards the base of the sequence, has been calculated as a function of fault Shale Gouge Ratio (SGR) using the relationships given by Manzocchi *et al.* (1999): SGR is the fraction of shale in the sequence which has passed each point on the fault (Yielding *et al.* 1997). The thickness of the faults is constant at 10 cm.

Three models are compared. In a fine-scale model, two phase fault-rock properties are attached explicitly to discrete grid blocks. Fault-rock properties have been generated as a function of fault permeability using the methods outlined earlier in the paper, with the difference that all the fault-rock, irrespective of its permeability, is assigned the same value of S_{wc}, and hence all fault-rock has identical relative permeability curves. This was done to decrease the simulation run times of the fine-scale simulation model. Three different imbibition fault-rock capillary curves are used depending on the fault permeability. Two coarse models both include the single phase transmissibility multiplier T_{abs}, but in one model the two phase fault-rock properties are included as pseudo-relative permeability curves attached to the upstream grid block, while in the other model they are ignored, as is conventional in flow simulation of faulted reservoirs. T_{abs} has been calculated based on the grid block dips, juxtaposition areas, net:gross ratios,

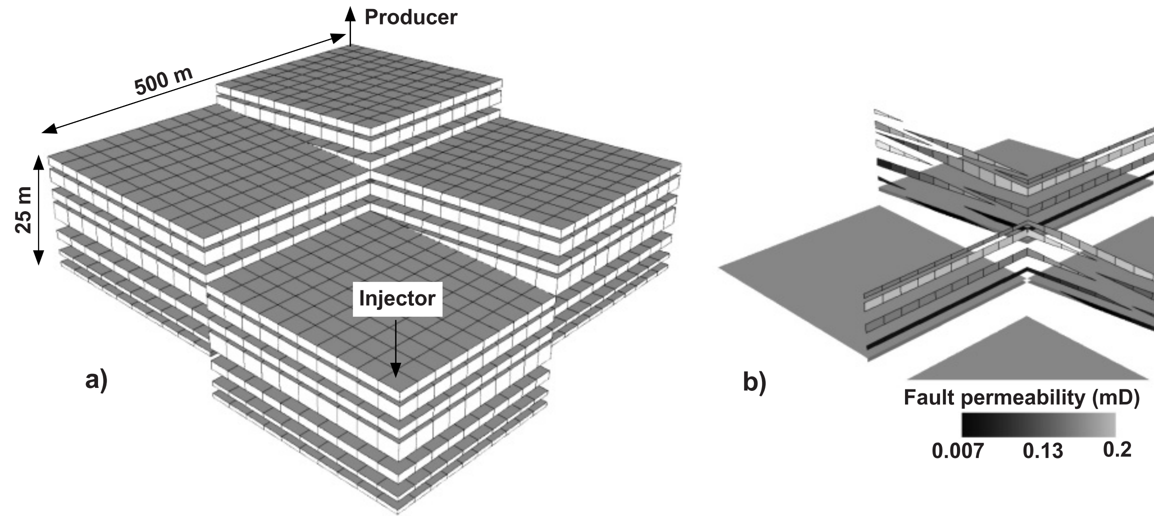

Fig. 10. Details of the 3D model used to test the methods developed for including two phase fault-rock properties. See text for discussion.

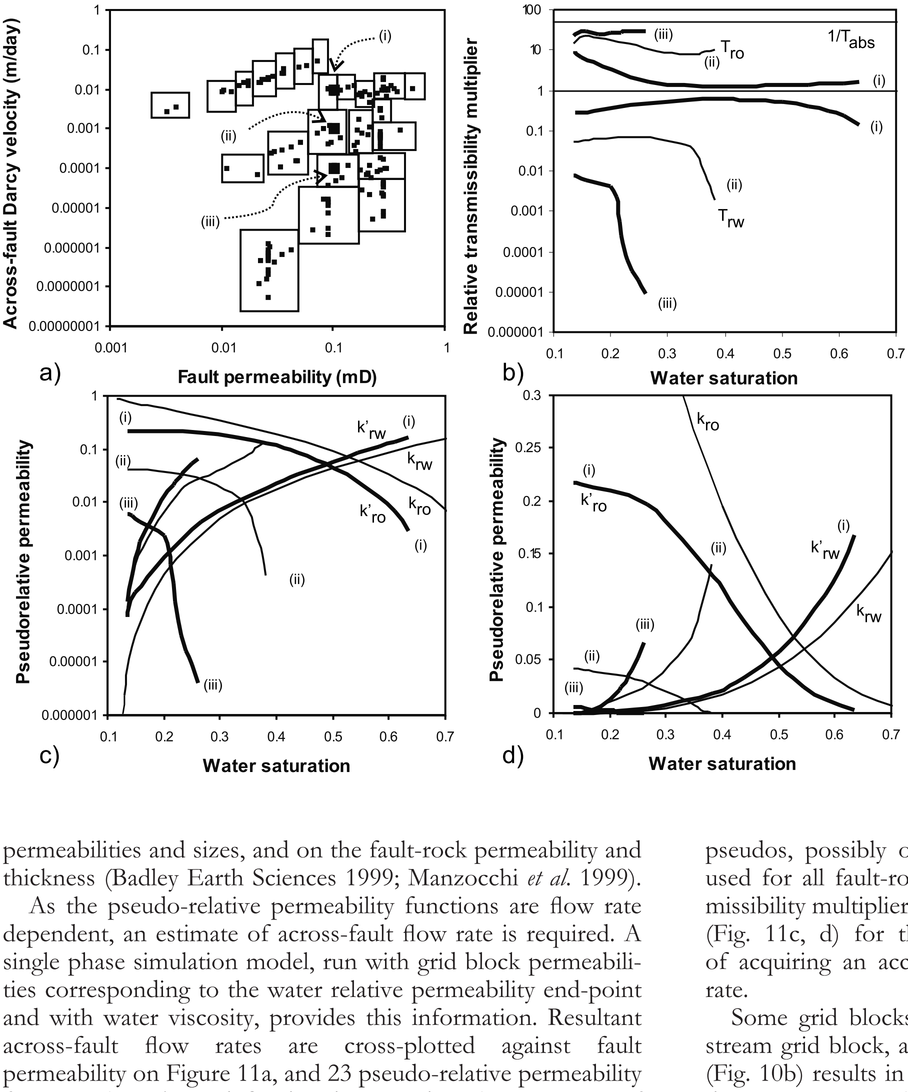

Fig. 11. (**a**) Across-fault Darcy velocity vs. fault permeability of each across-fault grid block to grid block connection, derived from a coarse scale, single phase flow simulation model. The boxes show the connection groupings assigned different pseudo-functions. The large squares represent the three different pseudos shown on (b)– (d). These all have 0.1 mD fault-rock and (i) 0.01, (ii) 0.001 and (iii) 0.0001 m day^{-1} across-fault Darcy velocities. (**b**) Relative transmissibility multipliers back-calculated from the pseudo-relative permeability functions, the latter are shown logarithmically in (**c**) and linearly in (**d**).

permeabilities and sizes, and on the fault-rock permeability and thickness (Badley Earth Sciences 1999; Manzocchi *et al.* 1999).

As the pseudo-relative permeability functions are flow rate dependent, an estimate of across-fault flow rate is required. A single phase simulation model, run with grid block permeabilities corresponding to the water relative permeability end-point and with water viscosity, provides this information. Resultant across-fault flow rates are cross-plotted against fault permeability on Figure 11a, and 23 pseudo-relative permeability functions have been defined and assigned to the groupings of connections shown on Figure 11a. This grouping has been made by eye; as noted by Christie (2001), defining optimal groupings of pseudo-functions is an unresolved pseudoization issue. Across-fault flow rate is found to be a much more significant variable than fault-rock permeability in these pseudos, possibly owing to the same saturation range being used for all fault-rock. The large differences in relative transmissibility multiplier (Fig. 11b) and pseudo-relative permeability (Fig. 11c, d) for three flow rates highlight the importance of acquiring an accurate description of the across-fault flow rate.

Some grid blocks are connected to more than one downstream grid block, and the variable throw on one of the faults (Fig. 10b) results in some layers in the two compartments that do not contain wells, being drained by flow paths from the injector or producer compartment in one layer and then back into the same compartment in another layer. Hence, in addition to acting as upstream grid blocks to connections with different across-fault flow rates, some grid blocks act simultaneously as upstream and downstream blocks across the same fault. This latter problem can be overcome by using directional irreversible pseudo-relative permeability functions (Schlumberger Geoquest 1999) which allow two sets of pseudo-functions per grid block per flow direction, so six different functions can define flow out of a six-faced upstream block. The problem of multiple connections downstream of a grid block is more problematic, and is similar to the problem, discussed by Manzocchi *et al.* (1999), associated with representing single phase fault properties as permeability multipliers attached to grid blocks, rather than as transmissibility multipliers attached to grid block to grid block connections. Where multiple downstream connections exist, the pseudo-function corresponding to the lowest across-fault flow rate has been used consistently in the model described.

Model results

Figure 12 shows four sets of water saturation maps from each representation of the model. In each case the top map is the fine-scale model with explicit two phase properties, the middle one is the representation including upstream grid block pseudos, and the bottom one is the comparison model using only T_{abs}: the conventional fault representation. Figure 12a shows the top layer injector compartment with oil trapped against the fault in the fine-scale model: this is well reproduced by the model including pseudos, but is absent from the model containing only T_{abs}. Figure 12b–d show all four compartments, and indicate that although in many layers the waterflood front is less advanced in the fine-scale model than in the model containing pseudos (e.g. Layer 3), this is not always the case (e.g. one of the compartments in Layer 7). In each case, however, the model containing pseudos provides a closer match to the fine-scale model than the conventional model containing only T_{abs}, in which the waterflood is consistently more advanced than either of the other representations.

The performances of the two wells throughout the simulation run are compared on Figure 13. The production rates (Fig. 13a) for the coarse pseudo-model (thicker curves) are roughly similar to those of the fine-scale model (crosses), particularly at later times, and consistently closer than the curves for the T_{abs} model (thinner curves). At early times the pseudo-model has higher oil production rates, complemented by higher water injection rates (Fig. 13b), than the fine-scale model. After about 30 years, the injection and production rates for the two models converge, and are approximately equal for the remainder of the simulation period. Thirty years corresponds to a time immediately prior to initial water breakthrough (Fig. 13a), and therefore to a time where the preferred flow paths from injector to producer have reasonably high water saturations over most of their length. At higher water saturations, the combined flow of the two phases (roughly proportional to the sum of the relative permeabilities normalized by the phase viscosities) approaches the flow rates in the water relative permeability end-point single phase simulation model, run to determine the across-fault flow rates contained in the pseudo-functions (Fig. 13c). At earlier times, when water saturations are lower, total flow rates are also lower (Fig. 13c), and therefore the pseudo-relative permeabilities are based on too high a flow rate for the saturations present. These observations are borne out by the well injection and production curves for the pseudo-model which show an overestimation of oil production at early times but an improved match in performance later in the simulation run.

In summary, this implementation has shown that when two phase fault-rock properties are included in faulted 3D flow models as pseudo-functions attached to the grid block upstream of a fault, an improved match to a fine-scale model with explicit two phase properties is obtained. Although there are problems concerning different flow rates out of a grid block into multiple downstream grid blocks, the greatest uncertainty in applying the method appears to be in determining appropriate across-fault flow rates. These flow rates are variable throughout a two phase simulation run (Fig. 13c), and therefore the pseudos should also vary. This problem is not particular to fault-rock pseudos, but is common to all two phase pseudoization exercises.

SUMMARY AND CONCLUSIONS

This study has been concerned with determining methods for including two phase fault-rock properties in conventional production flow simulation models, without representing the faults as discrete grid blocks. A comparison of available fault-rock and unfaulted sediment capillary pressure data indicates that fault-rocks and sediments with similar permeabilities have similar capillary threshold pressures. Therefore, in the absence of representative, ideally field-specific, fault-rock data, the fault-rock two phase properties may be estimated using the same methods used to estimate the two phase properties of sediments.

We have concentrated on faults in the imbibition cycle, which, in water-wet rock, have capillary pressure curves which go to zero at the irreducible oil saturation and therefore will contain both movable oil and movable water throughout a waterflood simulation. It is possible, however, that faults or portions of faults, particularly if they are close to the oil–water contact, do not contain movable oil as their capillary threshold pressures have not been reached. In this case the imbibition capillary pressure curve is inappropriate, and unless the reservoir conditions are altered during production such that the fault-rock capillary threshold pressures are exceeded, the faults will be total barriers to the flow of oil (but not water).

Using a 1D flow simulation model as an illustration, the closest two phase analogue of the single phase transmissibility multiplier has been determined. However, owing to the upstream relative permeability weighting used for the grid block to grid block flow calculations, the implementation of these multipliers is unnecessarily complex, as they depend on two well defined, but different, saturation averaging volumes. A more direct means of including the same information is by deriving relative permeability pseudo-functions which include the two phase fault-rock properties in the upstream grid block. A close two phase analogy of the single phase transmissibility multiplier is then given by the ratio of the pseudo-relative permeability to the unaltered grid block relative permeability. We have termed this ratio the relative transmissibility multiplier.

The relative transmissibility multiplier approximates to the ratio of phase-specific transmissibility multiplier normalized by the single phase transmissibility multiplier, and its form gives an indication of how closely the single phase multiplier would reproduce the two phase flow through the fault. In all cases we have examined, the water relative transmissibility multiplier lies in the range $1/T_{abs}>T_{rw}>1$ and the oil relative transmissibility multiplier lies in the range $1>T_{ro}>0$. If $T_{rp}=1$, the phase transmissibility multiplier is identical to the single phase multiplier (T_{abs}). Therefore these limits imply that T_{abs} is too restrictive to the flow of water, and too permissive to the flow of oil.

Relative transmissibility multipliers vary as a function of fault-rock permeability and thickness, grid block permeability, size, shape and net:gross ratio (these factors also influence the single phase transmissibility multiplier), as well as on the

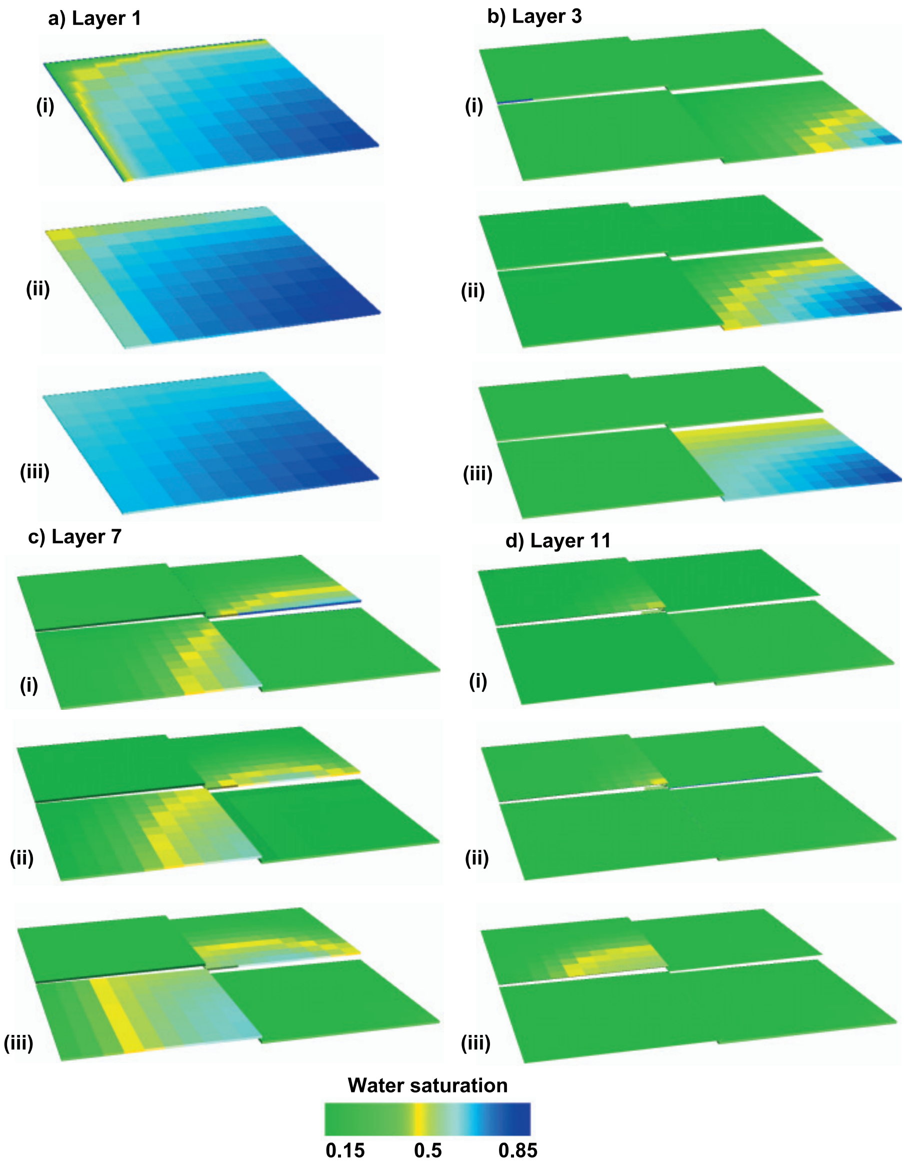

Fig. 12. Water saturation maps for different layers using the three different fault-rock representations, after 25 years. The water injector well is in the right-most grid block in each model: (**a**) top layer (Layer 1) for the compartment containing the injector well; (**b**) Layer 3; (**c**) Layer 7; (**d**) Layer 11. In each case, map (i) is for the fine model containing discrete two phase fault-rock properties, map (ii) is for the coarse model containing pseudo-relative permeability functions in grid blocks upstream of faults, and (iii) is for a coarse model containing only single phase transmissibility multipliers. Note that the injector-well compartment in Layers 7 and 11 are poorly connected or disconnected to the producer well (see Fig. 10), and hence oil saturation remains high in these compartments.

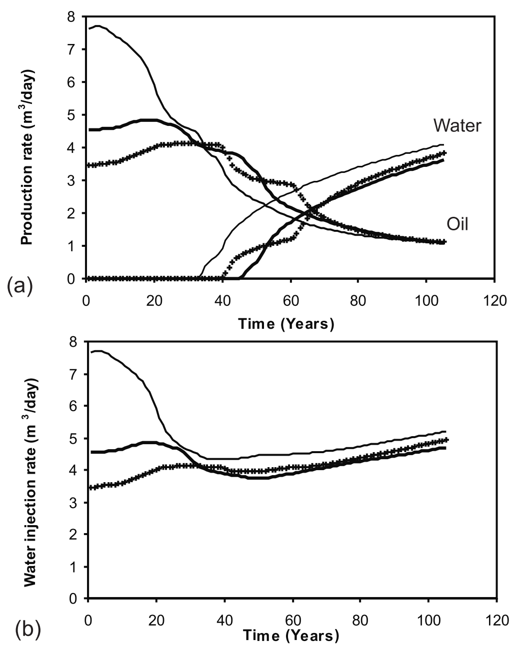

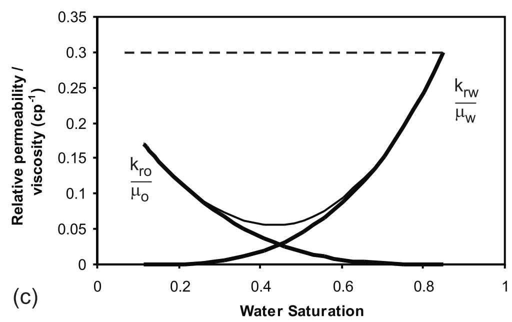

Fig. 13. Well performances for the three model representations: (**a**) water and oil production rate; (**b**) water injection rate. Crosses: fine model containing discrete two phase fault-rock properties. Thicker curves: coarse model containing pseudo-relative permeability functions in grid blocks upstream of faults. Thinner curves: coarse model containing only single phase transmissibility multipliers. (**c**) 1000 mD host-rock relative oil and water permeability curves, normalized by the phase viscosities (thicker curves). Across-fault flow rates are based on a single phase model with permeability set to the end-point water relative permeability and with water viscosity (horizontal line). The total across-fault flow rate is a function of the sum of k_{rp}/μ_p, shown by the thinner curve. See text for discussion.

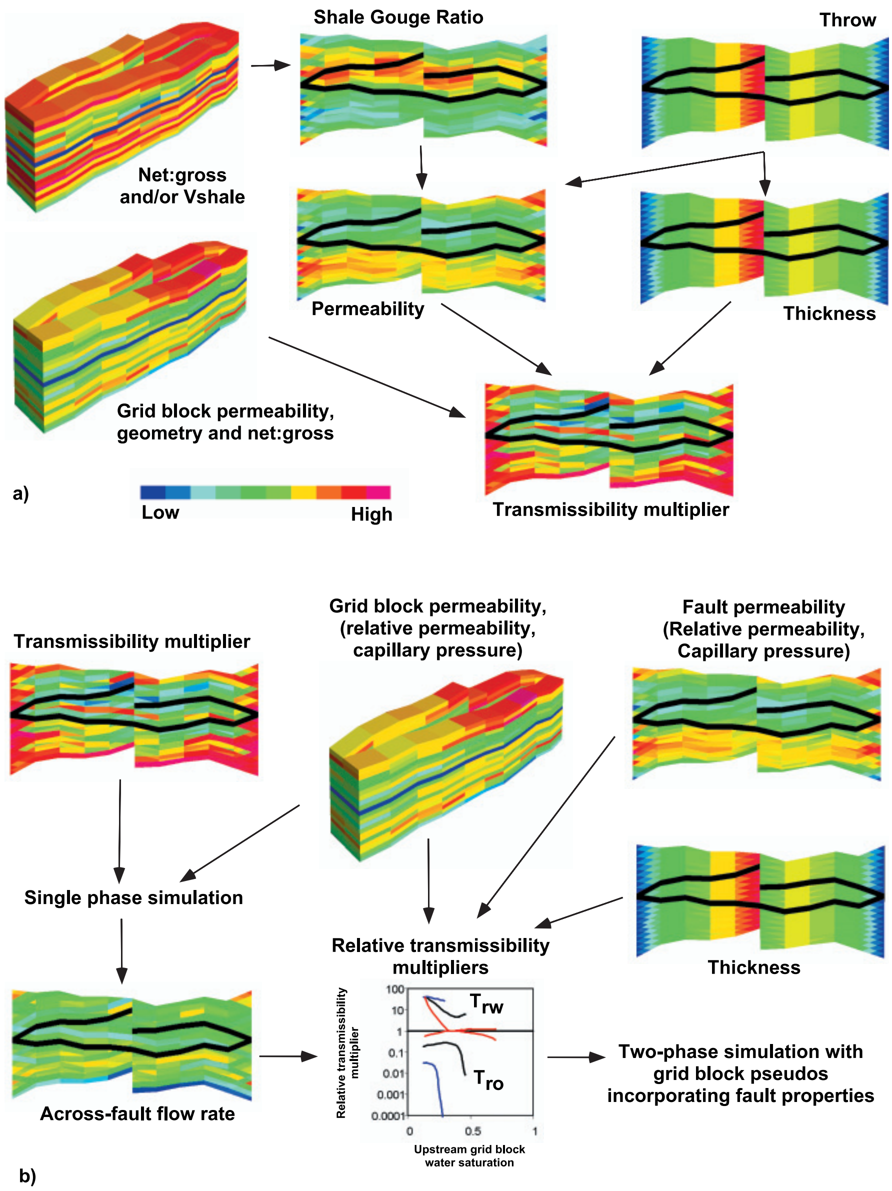

Fig. 14. Summary of a practical workflow for implementing two phase fault-rock properties in conventional flow simulation. (**a**) The workflow defined by Manzocchi *et al.* (1999) for incorporating geologically meaningful single phase transmissibility multipliers. Fault-rock permeability and thickness are calculated for each across-fault connection from field-specific empirical relationships linking permeability to Shale Gouge Ratio (SGR), and thickness to fault displacement. These variables are then combined with the permeabilities, geometries and net:gross ratios of the grid blocks to determine transmissibility multipliers for each across-fault connection. (**b**) Extension of this workflow for including two phase fault-rock properties. Fault-rock relative permeability and capillary pressure curves are determined as a function of the single phase fault-rock permeability predicted in (a), using the methods discussed in this paper. These are combined with across-fault flow rates defined from a single phase simulation run containing transmissibility multipliers. Representative relative transmissibility curves are then applied to the upstream grid blocks of groupings of across-fault connections sharing similar grid block properties, fault permeabilities, fault thickness and across-fault flow rates. These functions are combined with the grid block relative permeability curves to define the input required for full-field, two phase simulation of faulted reservoirs including two phase fault-rock properties.

relative permeability and capillary pressure curves of the fault-rock and host-rock, on the across-fault flow rates and on the fluid properties. We have examined the influence of only a few of these variables, but consider that in view of the geometrical simplicity of the pseudoization problem, which need only consider one coarse grid block and the fault-rock in one dimension, application of an optimal pseudoization scheme could fruitfully yield a comprehensive library of relative transmissibility multiplier functions which could be used to model routinely two phase effects of fault-rock in conventional production flow simulation.

We have examined pore volume weighted and Kyte & Berry pseudos. The Kyte & Berry approximation of the average (coarse) grid block pressures are more representative of the fine-scale model, hence Kyte & Berry pseudo-capillary pressures are more appropriate than pore volume weighted ones. For the example illustrated, the pseudo-relative permeabilities calculated using both methods are very similar, and gave a good match to the fine-scale models when used in conjunction with either the Kyte & Berry pseudo-capillary pressure or the unaltered coarse grid block capillary pressure. Although a good match was obtained in the example illustrated, we have experienced results which are less satisfactory, particularly in systems with larger grid blocks, narrower faults and stronger contrasts between grid block and fault-rock properties. Other pseudoization methods exist, and further work is needed to identify the optimal pseudoization method for these systems. One method which is potentially appealing is that of Dale *et al.* (1997), who showed that in 1D, an analytical solution exists for rate dependent steady state pseudo-relative permeability and capillary pressure functions, hence fine-scale flow simulation may not be necessary to determine the pseudos.

An implementation of the methods developed has been performed in a small 3D model containing a pair of faults producing non-trivial across-fault connection geometries and flow paths. The pore volume weighted pseudo-relative permeabilities went a long way towards reproducing the results obtained in a fine-scale model in which the two phase fault-rock properties are included discretely, and much of the remaining discrepancies are believed to be associated with the determination of the across-fault flow rate. 3D implementation problems exist in the situation where across-fault flow occurs at markedly different velocities from one grid block into two downstream grid blocks in the same direction. The problem can be reduced by refining the vertical resolution of the flow model, but will always be present in models containing realistic faults unless more than six directional relative permeability curves are allowed per grid block. Despite these caveats, we consider that inclusion of two phase fault-rock properties in conventional, faulted simulation models is feasible, and under certain circumstances may have a significant influence on the flow simulation results. A workflow for the routine inclusion of two phase properties in full-field flow simulation is sketched on Figure 14; this workflow is a generalization of that used in the 3D implementation described.

REFERENCES

Badley Earth Sciences 1999. *TransGen Version 1.0, Technical Description*.

Barker, J.W. & Dupouy, P. 1999. An analysis of dynamic pseudo-relative permeability methods for oil–water flows. *Petroleum Geoscience*, **5**, 385–394.

Barker, J.W. & Thibeau, S. 1997. A critical review of the use of pseudo-relative permeabilities for upscaling. *SPE Reservoir Engineering*, **May**, 138–143

Berg, R.R. & Avery, A.H. 1995. Sealing properties of Tertiary growth faults, Texas Gulf Coast. *American Association of Petroleum Geologists Bulletin*, **79**, 375–393.

Childs, C., Sylta, Ø., Moriya, S., Walsh, J.J. & Manzocchi, T. 2002. A method for including the capillary properties of faults in hydrocarbon migration models. *In:* Koestler, A.G. & Hunsdale, R. (eds) *Hydrocarbon Seal Quantification*. Norwegian Petroleum Society Special Publications, **11**.

Christie, M.A. 2001. Flow in porous media – scale up of multiphase flow. *Current Opinion in Colloid and Interface Science*, **6**, 236–241.

Corbett, P.W.M. & Jensen, J.L. 1993. Application of Probe Permeametry to The Prediction of 2-Phase Flow Performance in Laminated Sandstones (Lower Brent-Group, North-Sea). *Marine and Petroleum Geology*, **10**, 335–346.

Dale, M., Ekrann, S., Mykkeltveit, J. & Virnovsky, G. 1997. Effective relative permeabilities and capillary pressures for one-dimensional heterogeneous media. *Transport in porous media*, **26**, 229–260.

Evans, J.P., Forster, C.B. & Goddard, J.V. 1997. Permeability of fault-related rocks, implications for hydraulic structure of fault zones. *Journal of Structural Geology*, **19**, 1393–1404.

Faulkner, D.R. & Rutter, E.H. 1998. The gas permeability of clay-bearing fault gouges at 20° C. *In:* Jones, G., Fisher, Q.J. & Knipe, R.J. (eds) *Faulting, Fault Sealing and Fluid Flow in Hydrocarbon Reservoirs*. Geological Society, London, Special Publications, **147**, 147–156.

Fisher, Q.J. & Knipe, R.J. 1998. Fault sealing processes in siliciclastic sediments. *In:* Jones, G., Fisher, Q.J. & Knipe, R.J. (eds) *Faulting, Fault Sealing and Fluid Flow in Hydrocarbon Reservoirs*. Geological Society, London, Special Publications, **147**, 117–134.

Fowles, J. & Burley, S. 1994. Textural and permeability characteristics of faulted, high porosity sandstones. *Marine and Petroleum Geology*, **11**, 608–623.

Fristad, T., Groth, A., Yielding, G. & Freeman, B. 1997. Quantitative fault seal prediction – a case study from Oseberg Syd. *In:* Møller-Pedersen, P. & Koestler, A.G. (eds) *Hydrocarbon Seals: Importance for exploration and production*. Norwegian Petroleum Society Special Publications, **7**, 51–59.

Fulljames, J.R., Zijerveld, L.J.J. & Franssen, R.C.M.W. 1997. Fault seal process: systematic analysis of fault seals over geological and production time scales. *In:* Møller-Pedersen, P. & Koestler, A.G. (eds) *Hydrocarbon Seals: Importance for exploration and production*. Norwegian Petroleum Society Special Publications, **7**, 51–60.

Gibson, R.G. 1994. Fault zones seals in siliciclastic strata of the Columbus Basin, offshore Trinidad. *American Association of Petroleum Geologists Bulletin*, **78**, 1372–1385.

Gibson, R.G. 1998. Physical character and fluid flow properties of sandstone-derived fault zones. *In:* Coward, M.P., Daltaban, T.S. & Johnson, H. (eds) *Structural Geology in Reservoir Characterisation*. Geological Society, London, Special Publications, **127**, 83–98.

Harper, T.R. & Lundin, E.R. 1997. Fault seal analysis: reducing our dependence on empiricism. *In:* Møller-Pedersen, P. & Koestler, A.G. (eds) *Hydrocarbon Seals: Importance for exploration and production*. Norwegian Petroleum Society Special Publications, **7**, 149–164.

Heum, O.R. 1996. A fluid dynamic classification of hydrocarbon entrapment. *Petroleum Geoscience*, **2**, 145–158.

Ibrahim, M.A., Tek, M.R. & Katz, D.L. 1970. *Threshold pressure in gas storage*. American Gas Association, Arlington.

Knipe, R.J., Fisher, Q.J. & Jones, G. 1997. Fault seal analysis: successful methodologies, application and future directions. *In:* Møller-Pedersen, P. & Koestler, A.G. (eds) *Hydrocarbon Seals: Importance for exploration and production*. Norwegian Petroleum Society Special Publications, **7**, 15–38.

Kyte, J.R. & Berry, D.W. 1975. New pseudo functions to control numerical dispersion. *Journal of the Society of Petroleum Engineers*, **15**, 269–275.

Manzocchi, T., Ringrose, P.S. & Underhill, J.R. 1998. Flow through fault systems in high porosity sandstones. *In:* Coward, M.P., Johnson, H. & Daltaban, T. (eds) *Structural Geology in Reservoir Characterisation*. Geological Society, London, Special Publications, **127**, 65–82.

Manzocchi, T., Walsh, J.J., Nell, P. & Yielding, G. 1999. Fault transmissibility multipliers for flow simulation models. *Petroleum Geoscience*, **5**, 53–63.

Pittman, E.D. 1981. Effect of fault-related granulation on porosity and permeability of quartz sandstones Simpson Group (Ordovician), Oklahoma. *American Association of Petroleum Geologists Bulletin*, **65**, 2381–2387.

Ringrose, P.S., Sorbie, K.S., Corbett, P.W.M. & Jensen, J.L. 1993. Immiscible flow behaviour in laminated and cross-bedded sandstones. *Journal of Petroleum Science and Engineering*, **9**, 103–124.

Schlomer, S. & Krooss, B.M. 1999. Experimental characteristics of the hydrocarbon sealing efficiency of cap rocks. *Marine and Petroleum Geology*, **14**, 565–580.

Schlumberger Geoquest 1999. *Eclipse 100 Version 99A Technical Description*.

Schowalter, T.T. 1979. Mechanics of secondary hydrocarbon migration and entrapment. *American Association of Petroleum Geologists Bulletin*, **63**, 723–760.

Sperrevik, S., Gillespie, P.A., Fisher, Q.J., Halvorsen, T. & Knipe, R.J. 2002. Empirical estimation of fault-rock properties. *In:* Koestler, A.G. & Hunsdale, R. (eds) *Hydrocarbon Seal Quantification*. Norwegian Petroleum Society Special Publications, **11**.

Walsh, J.J., Watterson, J., Heath, A.E. & Childs, C. 1998. Representation and scaling of faults in fluid flow models. *Petroleum Geoscience*, **4**, 241–251.

Yielding, G., Freeman, B. & Needham, D.T. 1997. Quantitative fault seal prediction. *American Association of Petroleum Geologists Bulletin*, **81**, 897–917.

Yielding, G. 2002. Shale Gouge Ratio – calibration by geohistory. *In:* Koestler, A.G. & Hunsdale, R. (eds) *Hydrocarbon Seal Quantification*. Norwegian Petroleum Society Special Publications, **11**.

Received 8 June 2001; revised typescript accepted 28 March 2002